Volume 130, number 4 CHEMICAL PHYSICS LETTERS 10 October 1986

DETECTION OF THE SiH_2 RADICAL BY INTRACAVITY LASER ABSORPTION SPECTROSCOPY

J.J. O'BRIEN and G.H. ATKINSON

Department of Chemistry and Optical Sciences Center, University of Arizona, Tucson, AZ 85721, USA

Received 11 July 1986

The silylene radical, SiH_2, has been detected directly by absorption using intracavity laser spectroscopy under silane discharge conditions that produce silicon deposits. Rotationally resolved absorption spectra of the (020)–(000) and (010)–(000) vibronic bands in the $\tilde{A}\,^1B_1 \leftarrow \tilde{X}\,^1A_1$ transition of SiH_2 have been identified. The pressure of SiH_2 in these experiments approaches 20 mTorr. Other absorption lines have been observed including those associated with Ar I and Ar II transitions from the argon used to maintain the discharge and transitions from several electronically excited states of the H_2 formed as a product in the decomposition of silane.

1. Introduction

The fundamental importance of silicon chemistry in the manufacture of semiconductor materials has long motivated extensive studies of macroscopic conditions (e.g. the methods of decomposition of the source material, temperatures employed and flow dynamics) associated with the efficient chemical vapor deposition (CVD) of polycrystalline (Si) and amorphous silicon (a-Si:H) [1–12]. Most of this work has focused on the decomposition of silane (SiH_4) which has been the primary commercial source of deposited silicon films. A wide range of dissociation methods has been used including pyrolysis [1–7, 13], glow and radio-frequency discharges [8–10,14,15], and photolysis [11,12,16–20]. The molecular mechanism(s) underlying the CVD of Si and a-Si:H via any of these methods, however, remains to be firmly established and many quite different and often conflicting models have been developed to explain observed parameters of the CVD growth process [21–24].

Many of the molecular mechanisms proposed to account for CVD silicon chemistry are based on the gas chromatographic and mass spectroscopic analysis of stable end products formed during SiH_4 decomposition (e.g. refs. [15,18,19,25–27]) even though the critical chemical steps may occur during the initial stages of the process. It is only recently that several intermediate chemical species have been identified directly during the deposition process using mainly emission spectroscopy techniques [28–37]. Our current understanding of the reaction dynamics, however, remains so rudimentary that even the issue of whether Si deposition is determined primarily by homogeneous (gas phase) or heterogeneous (surface) reactions remains controversial [38–41].

An important experimental element in studying the gas phase decomposition of SiH_4 is the in situ, real-time detection of the primary dissociation products. Since several studies have indicated that silylene (SiH_2) is a dominant precursor to Si and a-Si:H deposition [5,6,15–20,25,39,40,42], its detection during SiH_4 dissociation is of special interest. The SiH_2 radical was first detected spectroscopically by transient absorption following the flash photolysis of phenylsilane [43]. The rotational analysis of the SiH_2 absorption spectrum obtained in the flash discharge of SiH_4 was subsequently reported [44,45]. These early studies were performed under experimental conditions optimized for maximum SiH_2 absorption which were not necessarily appropriate for CVD deposition of silicon films. Interest in monitoring SiH_2 during Si and a-Si:H deposition also has led to its detection by emission spectroscopy [46], coherent anti-Stokes Raman spectroscopy [47], laser-induced fluorescence (LIF) [48–50], and frequency-modulated absorption spectroscopy [51]. In these case, SiH_2 was produced by different methods including glow discharges in SiH_4 and disilane [51], ultraviolet photolysis of phenylsilane [48], and infrared multiphoton dissociation of SiH_4 and ethylsilane [46,49].

We report in this paper the detection of SiH_2 by absorption spectroscopy using the $\tilde{A}\,^1B_1 \leftarrow \tilde{X}\,^1A_1$ transitions near 579 nm and intracavity laser spectroscopy (ILS). ILS provides sufficiently high detection sensitivity to permit in situ, real-time measurements under experimental conditions appropriate for the deposition of Si and a-Si : H films. In addition to establishing its relative concentration, these ILS absorption spectra contain data on the internal energy distribution of SiH_2 and its spatial distribution in the reaction chamber. The SiH_2 radical is fomed by the microwave discharge of SiH_4 in argon.

2. Experimental

The optical and spectroscopic principles associated with ILS have been presented in detail elsewhere [52–55]. Briefly, enhanced sensitivity for detecting absorption is obtained by placing the molecular species of interest inside the optical resonator cavity of a multimode laser. Molecular and atomic absorptions contribute to the wavelength-dependent losses in the laser resonator as it approaches the threshold conditions for laser activity. The enhanced detection sensitivity can be quantitatively described in terms of the gain properties and mode competition associated with the resonator cavity [56]. The absorption spectra of the intracavity molecular and atomic species are superimposed on the output of the ILS laser. The absorption spectrum of a specific species can be identified and assigned when the output of the ILS laser is dispersed with respect to wavelength.

The ILS spectrometer is shown schematically in fig. 1. The ILS laser is a cw, jet-stream dye laser (Coherent 590) pumped by the 514.5 nm output of an argon ion laser operating at about 4 W (Coherent I-18). The pumping radiation is attenuated as a function of time by passing it through an acousto-optic modulator (AOM1). The AOM1 diverts enough pump power to prevent the dye laser from reaching thresh-

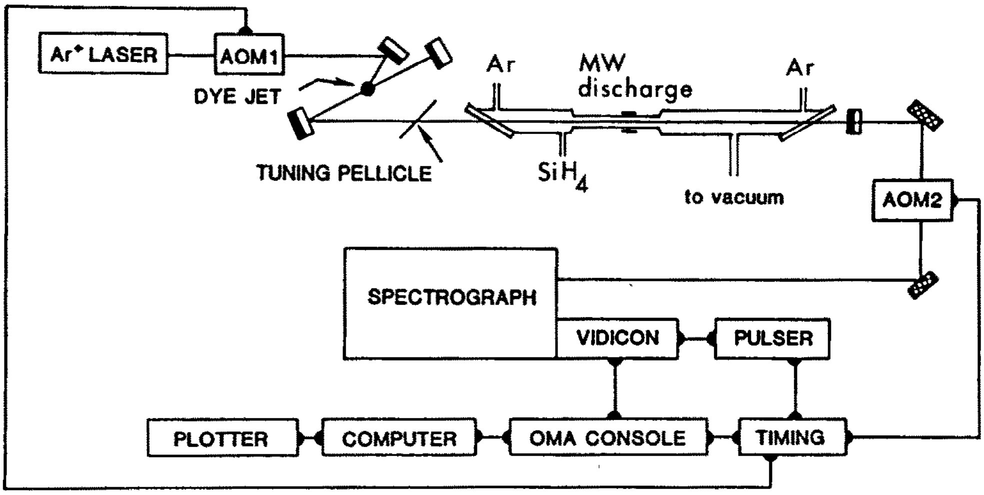

Fig. 1. Intracavity laser spectroscopy (ILS) system. The intensity of the argon ion laser pump beam is modulated in time by passage through an acousto-optic modulator (AOM1). When AOM1 is on, power is diverted from the pump beam to prevent the dye laser from attaining threshold conditions. When AOM2 is off, the dye laser is brought rapidly above laser threshold conditions. The sample chamber is contained within the optical resonator cavity of the dye laser. The sample chamber contains a section where the sample gas, silane, is dissociated by microwave discharge in an Evenson–Broida cavity. The output of the dye laser passes through AOM2 which diverts part of the output radiation into the spectrometer after the dye laser has been operating above threshold for a preset time. The wavelength-dispersed radiation is detected by an intensified vidicon camera.

old conditions. When AOM1 is switched off, the pump laser brings the dye laser rapidly above threshold. The dye laser output passes through a second acousto-optic modulator (AOM2) before entering an echelle spectrometer (McPherson model 2005). The time period during which the dye laser operates above threshold and the AOM2 remains open determines the generation time, t_g, of the ILS laser system [57]. The value of t_g controls the time interval over which the ILS absorption data are collected. In this work, t_g is typically 45 μs which, for a discharge to cavity length ratio of approximately 0.1, provides an equivalent pathlength of absorption of 1.35 km [54,55]. Longer generation times give stronger absorption signals than those presented here and equivalently permit the detection of transitions of weaker absorption strength.

The wavelength-dispersed radiation exiting the spectrometer is focused by a lens (50 mm focal length) onto the face of an intensified vidicon camera (PARC model 1205I). Such multichannel detection makes it feasible to monitor substantial portions of the rovibronic structure in the SiH_2 absorption spectrum in real time (i.e. 32.8 ms accumulation time of vidicon). This overall spectral resolution of the detection system is approximately 95000 (0.18 cm^{-1}). The spectral bandwidth of the ILS dye laser is 0.8 nm (22 cm^{-1}). The wavelength of the dye laser is controlled throughout the lasing range of the rhodamine 6G dye used by angle tuning an intracavity pellicle (uncoated).

The intracavity sample cell is constructed of quartz and fitted with 0.5 inch thick fused silica windows positioned at Brewster's angle. Silane was introduced into the sample cell by a stainless steel gas handling system at flow rates of 5–10 sccm. The inner surfaces of the cell windows were continuously flushed with argon to prevent contamination by particulate products of the discharge. Silane in argon was decomposed by a microwave discharge in an Evenson–Broida cavity operating at ≈100 W and in a geometry concentric with the laser axis. The microwave power supply was stabilized as reported previously [58].

3. Results

The wavelength-resolved output of the ILS dye laser operating with a microwave discharge of SiH_2 (1.4%) in argon at a total pressure of 1.1 Torr is shown in fig. 2C. For comparison, the ILS spectra obtained for a microwave discharge in (i) argon alone at 1 Torr total pressure and (ii) H_2 (9%) in argon at 0.17 Torr total pressure are presented in figs. 2A and 2B, respectively. The t_g values in these experiments are 49, 49 and 37 ms, respectively, and the total acquisition time for each is 10 s. It should be noted that the addition of H_2 to an argon discharge has the effect of reducing the intensities of the argon transitions (cf. spectra in figs. 2A and 2B).

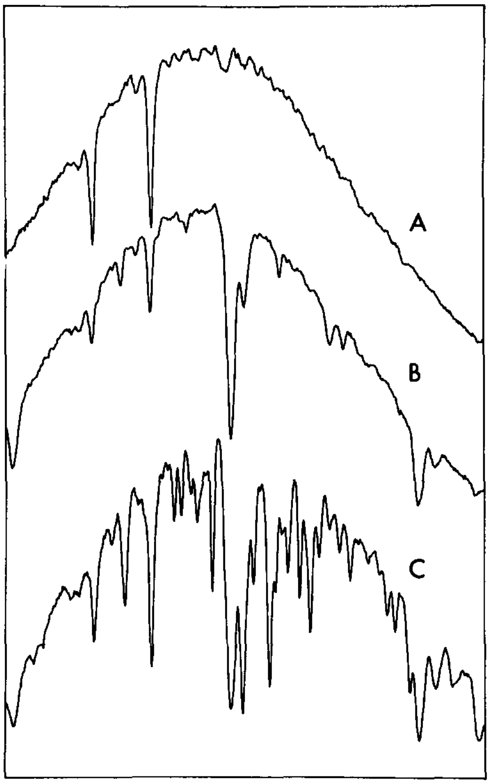

Fig. 2. The wavelength-resolved output of the ILS system for various microwave discharge conditions: (A) argon alone at 1 Torr pressure (t_g = 49 μs); (B) 9% H_2 in argon at 0.17 Torr pressure (t_g = 49 μs); (C) 1.4% SiH_4 in argon at 1.1 Torr pressure (t_g = 37 μs). These spectra of the laser profile are centered at 579.17 nm, extend for 0.75 nm and each took about 10 s to acquire.

Most of the absorption features observed in fig. 2C can be assigned to transitions between excited states of argon and H_2 or to $\tilde{A} \leftarrow \tilde{X}$ transitions in SiH_2. The argon absorptions are clearly identifiable from the ILS spectrum recorded for the pure argon sample and are assignable to either Ar I or Ar II. The argon lines

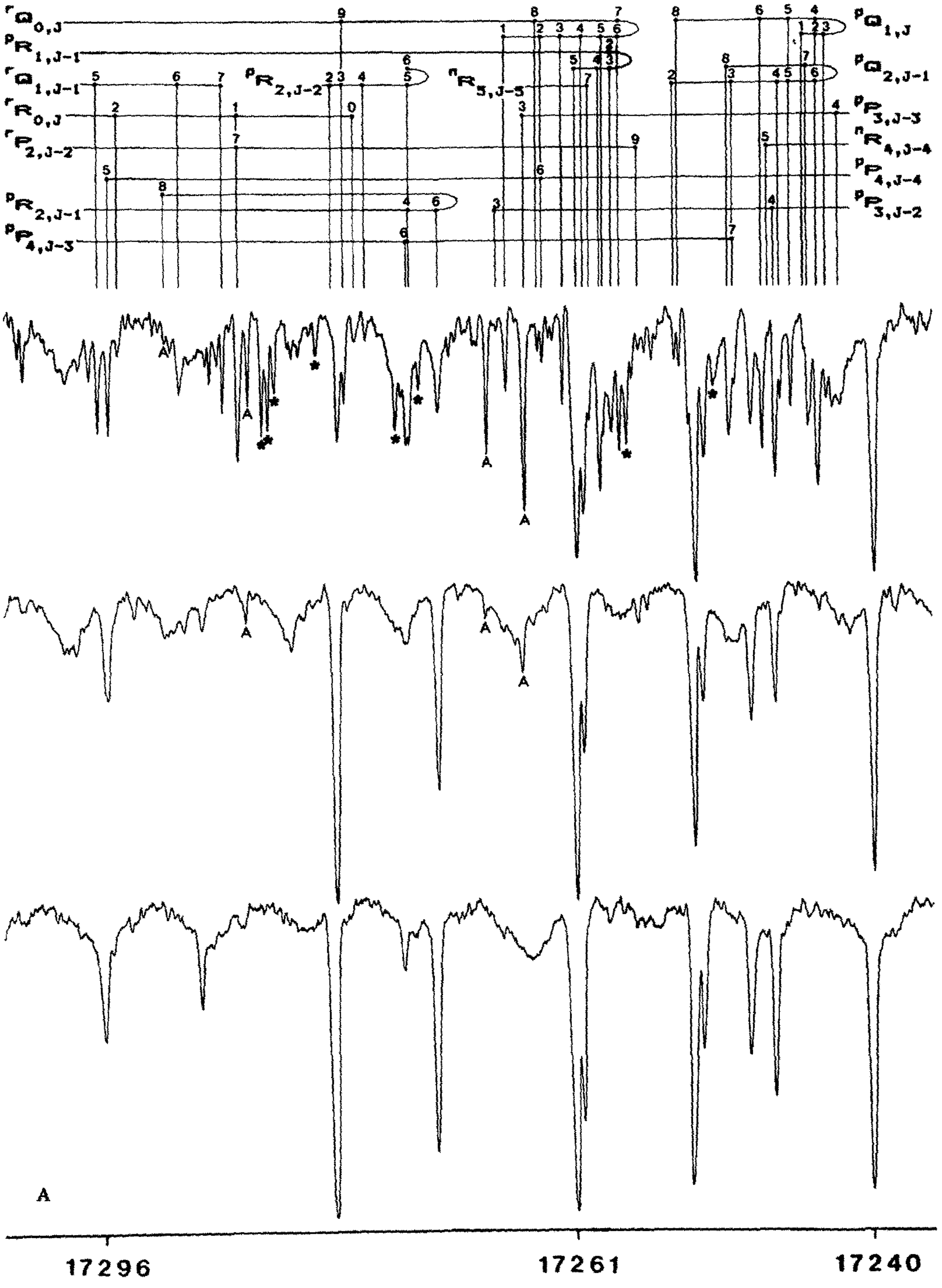
$^rQ_{0,J}$
$^pR_{1,J-1}$
$^rQ_{1,J-1}$
$^pR_{2,J-2}$
$^nR_{3,J-5}$
$^rR_{0,J}$
$^rP_{2,J-2}$
$^pR_{2,J-1}$
$^pP_{4,J-3}$
$^pQ_{1,J}$
$^pQ_{2,J-1}$
$^pP_{3,J-3}$
$^nR_{4,J-4}$
$^pP_{4,J-4}$
$^pP_{3,J-2}$
A
17296
17261
17240

Fig. 3 A.

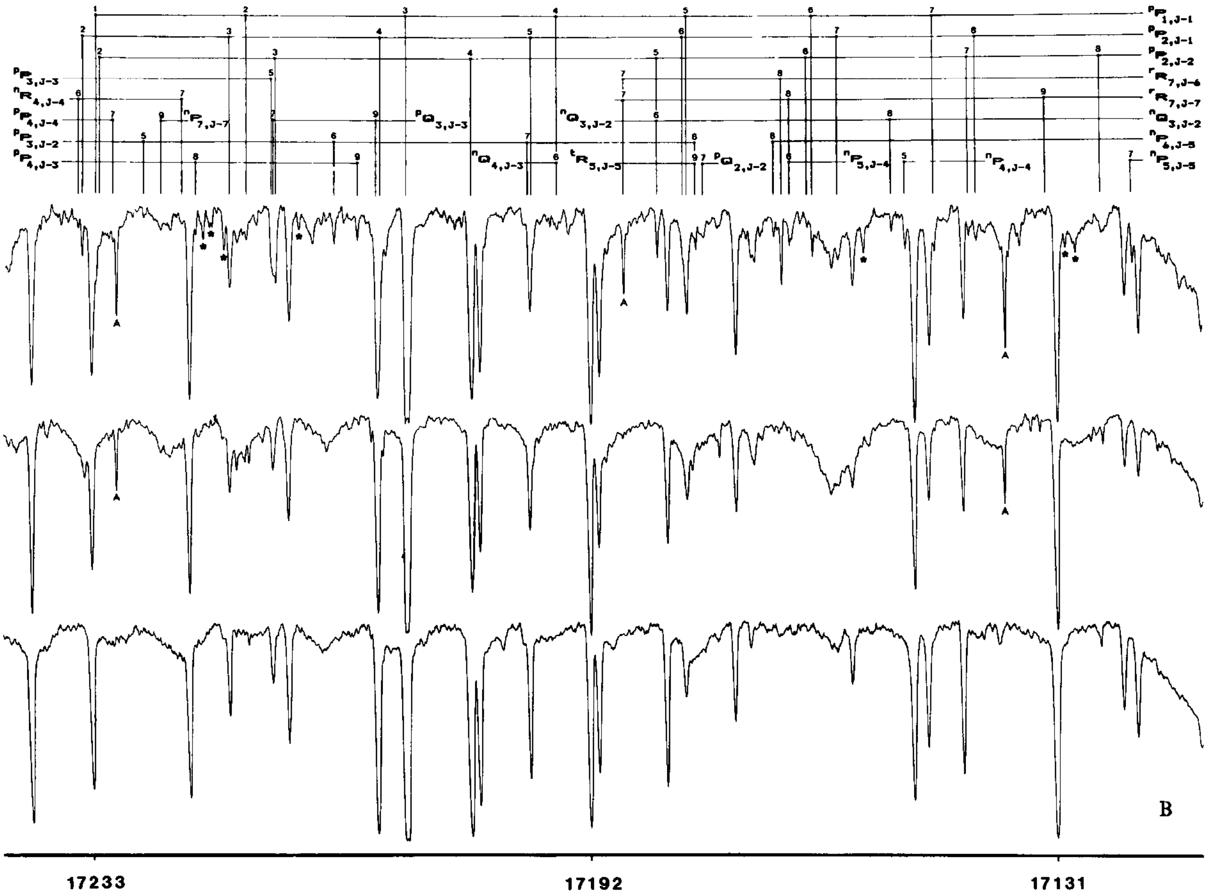

Fig. 3. ILS absorption spectrum of silylene, SiH_2, in the region of the $^1B_1$ (020)$-$$^1A_1$ (000) band (top). This spectrum was obtained from a 100 W microwave discharge of 4% SiH_4 in argon at a total pressure of 0.7 Torr. It is compared with spectra obtained from 100 W microwave discharges of 9% H_2 in argon at 0.17 Torr total pressure (middle) and 3% H_2 in helium at 0.17 Torr total pressure (bottom). These data were obtained by combining spectra, such as those shown in fig. 2, for 25 adjoining spectral regions. The assignment markers are for all the SiH_2 transitions in this spectral region that were listed by Dubois [62] and include several assignments from the (010)$-$(000) vibronic band ($^tR_{5,J-5}$ ($J = 9$), $^rR_{7,J-6}$ ($J = 7,8$), $^rR_{7,J-7}$ ($J = 7$–9). These data are presented in two panels (A, B) to highlight the region around 17261 cm^{-1} where the strongest SiH_2 transitions are observed. Note that the strongest bands observed are those due to excited-state–excited-state transitions in H_2 and that many of these bands overlap with features assigned to SiH_2.

shown in fig. 2A at 578.948 and 579.040 nm are assignable as the two Ar I transitions, 5d′ $[\frac{5}{2}]^o \leftarrow$ 4p$[\frac{3}{2}]$ and 7d$[\frac{1}{2}]^o \leftarrow$ 4p′ $[\frac{3}{2}]$, respectively [59]. The argon transitions serve as sources of spectral calibration for the other spectral features observed.

The five major absorption features due to H_2 in the ILS spectrum of the H_2/Ar discharge (fig. 2B) all appear in the ILS spectrum of the SiH_2/Ar discharge (fig. 2C). These five features can be assigned to transitions between electronically excited rotational levels of H_2 [60]. For example, the central absorption feature at 17261.3 cm^{-1} has been assigned in Dieke's notation [60] as the Q_3 rotational transition from the $v'' = 0$ vibrational level of the 2c excited electronic state (at 95392 cm^{-1}) to the $v' = 0$ vibrational level of the 3e excited electronic state. Several hundred other absorption features assignable to H_2 transitions have been observed in this study [61].

Table 1

Assignments and wavenumber positions of absorption transitions in the range 17242–17279 cm^{-1} for SiH_2 and excited-state argon and hydrogen (H_2) formed during the decomposition of SiH_4 in a microwave discharge [a]

SiH$_2$ transitions			Excited-state Ar and H$_2$ transitions		
assignments [b]	positions (vac. cm^{-1})		assignments [c,d]	positions (vac. cm^{-1})	
	published [b]	this work		published [c,d]	this work
			H_2: 3f 2–2c 2(R1) H_2: 4F 0–2B 9(R2)	17279.00	17279.17
${}^{p}R_{2,J-2}$ ($J = 3$) ${}^{r}Q_{0,J}$ ($J = 9$)	17278.45	17278.70			
${}^{r}R_{0,J}$ ($J = 0$)	17277.69	17277.92			
${}^{p}R_{2,J-2}$ ($J = 4$)	17276.86	17277.10			
${}^{p}P_{4,J-3}$ ($J = 6$)	17273.86	17273.89			
${}^{p}R_{2,J-2}$ ($J = 5$) ($J = 6$) ${}^{p}R_{2,J-1}$ ($J = 4$)	17273.64	17273.68			
${}^{p}R_{2,J-1}$ ($J = 6$)	17271.90	17271.86			
			H_2: 3f 0–2c 0(P3) H_2: unassigned	17271.54 17271.39	17271.53
			ArI: $\{5d'\ [\frac{5}{2}]^{o} \leftarrow 4p'\ [\frac{3}{2}]\}$	17267.92	used as ref.
${}^{p}P_{3,J-2}$ ($J = 3$)	17267.14				
${}^{r}Q_{0,J}$ ($J = 1$)	17266.47	17266.48			
			ArI: $\{7d\ [\frac{1}{2}]^{o} \leftarrow 4p'\ [\frac{3}{2}]\}$	17265.18	used as ref.
${}^{p}P_{3,J-3}$ ($J = 3$)	17265.23	17265.18	(overlap with Ar I transition)		
${}^{r}Q_{0,J}$ ($J = 8$)	17264.11	17264.15			
${}^{r}Q_{0,J}$ ($J = 2$) ${}^{p}P_{4,J-4}$ ($J = 6$)	17263.77	17263.80			
${}^{r}Q_{0,J}$ ($J = 3$)	17262.26	17262.28			
${}^{p}R_{1,J-1}$ ($J = 5$)	17261.70	17261.31	H_2: 3e 0–2c 0(Q3)	17261.31	17261.31
${}^{r}Q_{0,J}$ ($J = 4$)	17260.80	17260.82	H_2: 3e 0–2c 0(Q4)	17260.64	17260.82
${}^{n}R_{5,J-5}$ ($J = 7$)	17260.25	17260.13			
${}^{p}R_{1,J-1}$ ($J = 4$)	17259.92	17259.56			
${}^{r}Q_{0,J}$ ($J = 5$)	17259.50	17259.28			
${}^{p}R_{1,J-1}$ ($J = 2$) ($J = 3$)	17258.89 17258.63	17258.68			
${}^{r}Q_{0,J}$ ($J = 6$) ($J = 7$)	17258.05	17257.79			
${}^{r}P_{2,J-2}$ ($J = 9$)	17256.68	17256.42			
${}^{p}Q_{2,J-1}$ ($J = 2$)	17253.98	17253.76			
${}^{p}Q_{1,J}$ ($J = 8$)	17253.01	17253.43			
			H_2: 3e 0–2c 0(Q5)	17252.63	17252.38
			H_2: 3f 0–2c 0(P4)	17251.88	17251.70
${}^{p}Q_{2,J-1}$ ($J = 8$)	17250.07	17249.70			
${}^{p}P_{4,J-3}$ ($J = 7$) ${}^{p}Q_{2,J-1}$ ($J = 3$)	17249.71	17249.30			
			H_2: 3e 0–2c 0(Q2)	17248.52	17248.11
${}^{p}Q_{1,J}$ ($J = 6$)	17247.65	17247.22			
${}^{r}R_{4,J-4}$ ($J = 5$)	17248.18	–			
${}^{p}P_{3,J-2}$ ($J = 4$)	17246.78	17246.33	H_2: 3f 2–2c 2(Q5) H_2: 3E 0–2B 4(R3)	17246.69	17246.33
${}^{p}Q_{2,J-1}$ ($J = 4$)	17246.30	17245.91			
${}^{p}Q_{1,J}$ ($J = 5$) ${}^{p}Q_{2,J-1}$ ($J = 5$)	17245.52	17245.14			

Table 1 (continued)

SiH_2 transitions				Excited-state Ar and H_2 transitions		
assignments [b]		positions (vac. cm^{-1})		assignments [c,d]	positions (vac. cm^{-1})	
		published [b]	this work		published [c,d]	this work
$^{P}Q_{1,J}$	$(J = 1)$	17244.56	17244.17			
$^{P}Q_{2,J-1}$	$(J = 7)$	17244.15	17243.88			
$^{P}Q_{1,J}$	$(J = 2)$	17243.61	17243.20			
$^{P}Q_{2,J-1}$	$(J = 6)$	17243.59				
$^{P}Q_{1,J}$	$(J = 4)$	17243.55				
	$(J = 3)$	17242.92	17242.53			

[a] Transitions measured from the same segment (e.g. fig. 2C) of the composite spectrum (fig. 3A) are grouped together.
[b] From ref. [62]. [c] From ref. [59] for Ar transition positions.
[d] From ref. [60] for H_2 transition positions.

Most of the absorption features appearing in the spectrum of the SiH_4/Ar discharge (fig. 2C) that cannot be attributed to either Ar or H_2 are assignable to rotational transitions in the (0,2,0)–(0,0,0) band of SiH_2 [44,62]. The complete absorption spectrum of the (0,2,0)–(0,0,0) band of SiH_2 can be obtained by combining the spectral region observed in each ILS experiment (e.g. the segment in fig. 2A) with those at adjacent wavelengths. The result for combining 25 such segments around 579.6 nm is presented in figs. 3A and 3B for a microwave discharge (160 W) through 4% silane in argon at a total pressure of 0.7 Torr. Analogous ILS absorption spectra are presented for microwave discharges (160 W) through 9% H_2 in argon and 3% H_2 in helium are also presented in figs. 3A and 3B. The total pressure in these latter two experiments was 0.17 Torr. The assignments shown are all those listed for this spectral region by Dubois [62] and include several rotational transitions in the (010)–(000) band of SiH_2. Absorption bands that appear in discharges of argon alone are labeled as A. In some cases, these argon lines overlap SiH_2 features. Such overlapping has been verified by ILS spectra obtained from discharges of silane in helium. Several relatively intense bands that cannot be attributed to the presence of argon or hydrogen and that do not correspond to any of the bands listed in the tables of Dubois as assignable to SiH_2 are labeled with asterisks. The relative intensities observed within a rotational branch agree qualitatively with those reported by Dubois [62].

The frequency positions observed for all SiH_2 transitions in the 17279–17242 cm^{-1} region of fig. 3A are compared with those reported by Dubois [62] in table 1. The frequency positions observed for the strong excited-state – excited-state H_2 transitions that occur in this region are also compared in table 1 with those in the compilation of Dieke [60]. All transitions derived from one segment (i.e. fig. 2C) of the composite spectrum are grouped together in table 1. Where an argon transition is present in a given segment, it is used as primary frequency standard. Otherwise, a more general procedure based on a series of measurements of argon transition frequencies and linear interpolation between them is adopted for frequency calibration. Frequencies also have been corrected for the changing spectral dispersion of the detection system.

4. Discussion

The identification of SiH_2 in the microwave discharge of the SiH_4 in Ar mixture is evident from the absorption assignment presented in figs. 3A and 3B and in table 1. This is particularly clear in the 17261.3 cm^{-1} region (fig. 3A). Ambiguities in assignments caused by the overlap of absorption features from Ar, H_2, and SiH_2 can be resolved through comparisons between the ILS spectra presented here. Nonetheless, examination of the published rotational analysis of SiH_2 [44,62] suggests that such overlapping transitions, if present, may not have been completely separated in previous work. There are significant discrepancies between the spectroscopically observed levels of SiH_2 and those predicted from the rotational constants obtained in the published analysis [44]. Transitions due to excited state absorption transitions in H_2 may have been mistakenly assigned to SiH_2 and subsequently used in the rotational analysis. The opportunity to clearly distinguish these two sources of absorption lines afforded by ILS suggests that the rotational analysis of SiH_2 should now be reexamined in order to obtain more accurate rotational constants [61].

The electronically excited argon and H_2 species that are spectroscopically observed indicate that the energy of the microwave discharge is at least 13.3 eV. There are numerous SiH_4 decomposition pathways accessible at these energies including [15]:

$$
\begin{aligned}
SiH_4 + e^- &\rightarrow SiH_2 + H_2 + e^- && (2.43\ \text{eV}), && \text{(a)}\\
&\rightarrow SiH_3 + H + e^- && (3.86\ \text{eV}), && \text{(b)}\\
&\rightarrow SiH_2 + e^- && (6.74\ \text{eV}), && \text{(c)}\\
&\rightarrow SiH_2^+ + H_2 + 2e^- && (11.9\ \text{eV}), && \text{(d)}\\
&\rightarrow SiH_3^+ + H + 2e^- && (12.3\ \text{eV}). && \text{(e)}
\end{aligned}
$$

The 147 nm photolysis of silane utilizes 8.4 eV photons and has been shown to proceed via reactions (b) and (c) with quantum yields of 0.17 and 0.83, respectively [18]. The H_2 product is thought to be generated alos in a rapid secondary reaction [63]:

$$H + SiH_4 \rightarrow H_2 + SiH_3 \,. \qquad \text{(f)}$$

In view of the large number of processes that generate H_2, the prevalence of excited-state H_2 transitions in the ILS spectrum presented here is not surprising. Indeed, most of the absorption spectroscopy reported here (with the exception of the bands labelled by asterisks in figs. 3A and 3B) can be interpreted in terms of the decomposition of silane and the secondary excitation of a product of the primary decomposition step, H_2.

The detection of SiH_2 by ILS provides several advantages which should be noted.

(i) The detection sensitivity is sufficiently high to permit direct, in situ monitoring under the experimental conditions required for CVD of Si and a-Si : H films.

(ii) The broad spectral regions observable make it feasible to obtain rotational analyses of the absorption spectra, thereby unequivocably identifying the SiH_2 radical. Such analyses also permit the identification of as yet undetected species (e.g. SiH_3).

(iii) ILS data contain information on the spatial distribution of absorbing species in a reaction chamber.

(iv) Detection measurements are rapid enough to provide a basis for real-time optimization of the condition for SiH_4 decomposition.

(v) ILS data can be obtained under decomposition conditions that do not produce a suitable environment for the application of other sensitive detection techniques such as LIF and photoacoustic absorption spectroscopy.

These features suggest that ILS can have an important impact on our understanding of silicon chemistry.

Acknowledgement

The authors wish to thank Dr. N. Goldstein for technical assistance and Professor P. Bernath for helpful discussions concerning spectroscopic assignments. This work received partial support from the IBM Corp. and the University of Arizona.

References

[1] A.M. Beers and J. Bloem, Appl. Phys. Letters 41 (1982) 153.

[2] P. Hey and B.O. Seraphin, Solar Energy Materials 8 (1982) 215.

[3] W.A. Bryant, Thin Solid Films 60 (1979) 19.

[4] M. Meunier, J.H. Flint, D. Adler and J.S. Haggerty, J. Non-Cryst. Solids 59/60 (1983) 699.

[5] B.A. Scott, M.H. Brodsky, D.C. Green, P.B. Kirby, R.M. Plecenik and E.E. Simonyi, Appl. Phys. Letters 37 (1980) 725.

[6] B.A. Scott, R.M. Plecenik and E.E. Simonyi, Appl. Phys. Letters 39 (1981) 73.

[7] B.A. Scott, W.L. Olbricht, J.A. Reimer, B.S. Meyerson and D.J. Wolford, J. Non-Cryst. Solids 59 /60 (1983) 659.

[8] B. Drevillon, J. Huc, A. Lloret, J. Perrin, G. de Rosny and J.P.M. Schmitt, Appl. Phys. Letters 37 (1980) 646.

[9] S.R. Mejia, R.D. McLeod, K.C. Kao and H.C. Card, J. Non-Cryst. Solids 59/60 (1983) 727.

[10] O. Kuboi, M. Hashimoto, Y. Yatsurugi, H. Nagai, M. Aratani, M. Yanokura, S. Hayashi, I. Kohno and T. Nozaki, Appl. Phys. Letters 45 (1984) 543.

[11] C.P. Christensen and K.M. Lakin, Appl. Phys. Letters, 32 (1978) 254.

[12] M. Hanabusa, A. Namiki and K. Yoshihara, Appl. Phys. Letters 35 (1979) 626.

[13] J. Steinwandel and J. Hoeschele, Chem. Phys. Letters 116 (1985) 25.

[14] T. Hamasaki, M. Ueda, M. Hirose and Y. Osaka, J. Non-Cryst. Solids 59 /60 (1983) 679.

[15] P.A. Longeway, R.D. Estes and H.A. Weakliem, J. Phys. Chem. 88 (1984) 73.

[16] M.A. Ring, G.D. Beverly, F.H. Koester and R.P. Hollandsworth, Inorg. Chem. 8 (1969) 2033.

[17] T.F. Deutsch, J. Chem. Phys. 70 (1979) 1187.

[18] G.C.A. Perkins, E.R. Austin and F.W. Lampe, J. Am. Chem. Soc. 101 (1979) 1109.

[19] P.A. Longeway and F.W. Lampe, J. Am. Chem. Soc. 103 (1981) 6813.

[20] P.A. Longeway and F.W. Lampe, J. Phys. Chem. 87 (1983) 354.

[21] F. Hottier and R. Cadoret, J. Cryst. Growth 52 (1981) 199.

[22] J. Korec and M. Heyen, J. Cryst. Growth 60 (1982) 286.

[23] W.A.P. Claassen, J. Bloem, W.G.J.N. Valkenburg and C.H.J. van der Brekel, J. Cryst. Growth 57 (1982) 259.

[24] M.E. Coltrin, R.J. Kee and J.A. Miller, J. Electrochem. Soc. 131 (1984) 425.

[25] J.H. Purnell and R. Walsh, Proc. Roy. Soc. A293 (1966) 543.

[26] I. Haller, Appl. Phys. Letters 37 (1980) 282.

[27] R. Robertson, D. Hils, H. Chatham and A. Gallagher, Appl. Phys. Letters 43 (1983) 544.

[28] J. Perrin and E. Delafosse, J. Phys. D13 (1980) 759.

[29] F.J. Kampas and R.W. Griffith, J. Appl. Phys. 52 (1981) 1285.

[30] J.C. Knights, J.P.M. Schmitt, J. Perrin and G. Guelachvili, J. Chem. Phys. 76 (1982) 3414.

[31] A. Matsuda and K. Tanaka, Thin Solid Films 92 (1982) 171.

[32] H.U. Lee, J.P. Deneufville and S.R. Ovshinsky, J. Non-Cryst. Solids 59/60 (1983) 671.

[33] F.J. Kampas and R.R. Corderman, J. Non-Cryst. Solids 59/60 (1983) 683.

[34] P. Ho and W.G. Breiland, Appl. Phys. Letters 44 (1983) 51.

[35] J.P.M. Schmitt, P. Gressier, M. Krishnan, G. de Rosny and J. Perrin, Chem. Phys. 84 (1984) 281.

[36] R.M. Roth, K.G. Spears and G. Wong, Appl. Phys. Letters 45 (1984) 28.

[37] P.B. Davies, N.A. Isaacs, S.A. Johnson and D.K. Russell, J. Chem. Phys. 83 (1985) 2060.

[38] R. Robertson, D. Hils and A. Gallagher, Chem. Phys. Letters 103 (1984) 397.

[39] H.E. O'Neal and M.A. Ring, Chem. Phys. Letters 107 (1984) 442.

[40] J.H. Purnell and R. Walsh, Chem. Phys. Letters 110 (1984) 330.

[41] J.M. Jasinski and R.D. Estes, Chem. Phys. Letters 117 (1985) 495.

[42] J.S. Francisco, S.A. Joyce, J.I. Steinfeld and F. Walsh, J. Phys. Chem. 88 (1984) 3098.

[43] I. Dubois, G. Herzberg and R.D. Verma, J. Chem. Phys. 47 (1967) 4262.

[44] I. Dubois, Can. J. Phys. 46 (1968) 2485.

[45] I. Dubois, G. Duxbury and R.N. Dixon, J. Chem. Soc. Faraday Trans. II 71 (1975) 799.

[46] J.F. O'Keefe and F.W. Lampe, Appl. Phys. Letters 42 (1983) 217.

[47] N. Hata, A. Matsuda and K. Tanaka, J. Non-Cryst. Solids 59 /60 (1983) 667.

[48] G. Inoue and M. Suzuki, Chem. Phys. Letters 105 (1984) 641.

[49] D.M. Rayner, R.P. Steer, P.A. Hackett, C.L. Wilson and P. John, Chem. Phys. Letters 123 (1986) 449.

[50] J.M. Jasinski, J. Phys. Chem. 90 (1986) 555.

[51] J.M. Jasinski, E.A. Whittaker, G.C. Bjorklund, R.W. Dreyfus, R.D. Estes and R.E. Walkup, Appl. Phys. Letters 44 (1984) 1155.

[52] G.H. Atkinson, A.H. Laufer and M.J. Kurylo, J. Chem. Phys. 59 (1973) 350.

[53] G.H. Atkinson, T.N. Heimlick and M.W. Schuyler, J. Chem. Phys. 66 (1977) 5005.

[54] F. Stoeckel, M.A. Melieres and M. Chenevier, J. Chem. Phys. 76 (1982) 2191.

[55] M. Chenevier, M.A. Melieres and F. Stoeckel, Opt. Commun. 45 (1983) 385.

[56] F. Stoeckel and G.H. Atkinson, Appl. Opt. 24 (1985) 3591.

[57] N. Goldstein, T.L. Brack and G.H. Atkinson, Chem. Phys. Letters 116 (1985) 223.

[58] G.H. Atkinson, M.E. McIlwain, C.G. Venkatesh and D.M. Chapman, J. Photochem. 8 (1978) 307.

[59] W.L. Wiese, M.W. Smith and B.M. Miles, eds., Atomic transition probabilities. Vol. 2. Sodium through calcium, A. Critical data compilation, NSRDS-NBS 22 (1969).

[60] H.M. Crosswhite, ed., The hydrogen molecule wavelength tables of Gerhard Heinrick Dieke (Wiley–Interscience, New York, 1972).

[61] J.J. O'Brien and G.H. Atkinson, unpublished results.

[62] I. Dubois, Depository for Unpublished Data, National Science Library, Ottawa, Canada.

[63] E.R. Austin and F.W. Lampe, J. Phys. Chem. 81 (1977) 1134.